SPACE TELESCOPE SCIENCE INSTITUTE
Operated for NASA by AURA

Instrument Science Report STIS 2012-01

Post-SM4 Sensitivity Calibration of the STIS Echelle Modes

K. Azalee Bostroem[1], A. Aloisi[1], R. Bohlin[1], P. Hodge[1], C. Proffitt[1,2]

[1] Space Telescope Science Institute, Baltimore, MD [1] Computer Science Corporation, Baltimore, MD

January 30, 2012

ABSTRACT

On-orbit sensitivity curves for all echelle modes were derived for post - servicing mission 4 data using observations of the DA white dwarf G191-B2B. Additionally, new echelle ripple tables and grating dependent bad pixel tables were created for the FUV and NUV MAMA. We review the procedures used to derive the adopted throughputs and implement them in the pipeline as well as the motivation for the modification of the additional reference files and pipeline procedures.

Contents

1. Introduction

The Space Telescope Imaging Spectrograph (STIS) has four cross-dispersed echelle modes: E140H, E140M, E230H, and E230M which provide spectroscopic coverage from 1150 Å to 3100 Å at resolving powers of R $\sim$ 25,000-45,000 for the medium-resolution modes and R $\sim$ 110,000 for the high-resolution modes. Providing simultaneous observations of multiple orders, these modes are designed to maximize both the spectral coverage achieved in a single exposure and the resolution of a point source.

An initial flux calibration of the 12 prime echelle medium- and high-resolution modes was presented in Bohlin (1998). A new calibration of all echelle modes was completed in 2006 (Aloisi et al. 2007) for the final calibration of the STIS archival data following the instrument's failure in 2004. This analysis benefits from many improvements to the calibration of STIS data, most importantly a 2-D algorithm for removing scattered light from background measurements (Valenti et al. 2002), a characterization of the changes in sensitivity with time (Stys et al. 2004; Aloisi et al, 2007; Aloisi et al, 2011), and a characterization of the behavior of the echelle blaze function (Aloisi et al. 2005; see also Appendix A for more details).

STIS was successfully repaired during Servicing Mission 4 (SM4) in May 2009. Extrapolation over the length of time since the creation of the PHT table amplifies any error in the determination of the flux due to uncertainties in the time dependent sensitivity calibration as well as the temporal component of the blaze function shift. Additionally, the behavior of the blaze function shift changed with the switch from Side-1 to Side-2 electronics in mid-2001. After STIS was revived during SM4, another such change was anticipated. For these reasons the Cycle 17 program 11866 was undertaken to observe all STIS echelle modes and derive a new sensitivity calibration for post-SM4 data.

In this ISR we present the on-orbit sensitivity calibration of all echelle primary and secondary modes for post-SM4 data. This process has lead to improvements in the **calstis** pipeline and the creation of new reference files which will also be detailed here.

2. Observations

All observations in program 11866 were taken of the HST Primary Standard White Dwarf G191-B2B. Exposure times were chosen to achieve a peak S/N ratio of 30 per resolution element for E140M, E140H, and E230M and a peak S/N ratio of 20 per

resolution element for E230H. Additionally, the most commonly used Cycle 17 far ultraviolet (FUV) modes (E140H/1234, E140M/1425, and E140H/1343) were observed to obtain a peak S/N ratio of 100. Visit 03 was repeated due to a guide star failure. All data were obtained between November 28, 2009 and January 6, 2010. The standard echelle aperture of 0.2″x 0.2″was used.

In August 2002 the mode select mechanism (MSM) offsetting discontinued for all echelle observations. For the data taken in 11866 (unlike previous programs) the MSM offsetting was at the nominal position for all observations.

2.1 Echelle Flux Anomaly

Following SM4, the time-dependent sensitivity (TDS) of most STIS modes continued their pre-failure trends. However, the September 2009 observations of the HST standard White Dwarf BD+284211 with the E140H/1416 and E230M/2707 grating showed anomalously low throughputs (10-15% and 5% respectively). The next observation of the same star occurred in April 2010 and the anomaly appears to be gone. The STIS MAMA high-voltage power supplies were shut down from mid-September 2010 to mid-November 2010. The November 2010 observation of BD+284211 with the E140H shows a similar (although smaller) effect. While the effect appears to be related to the shutdown of the detectors, it has not otherwise been characterized.

As the data from 11866 were taken after the anomaly first occurred in the data and before the confirmation of its disappearance, there was some concern that our data may have been compromised. Part of the testing of the new PHT tables was to calibrate all of the TDS monitoring data (from September 2009 to August 2011) with the new reference files. If the anomaly were present in the files used to create the PHT tables, the calibrated flux of these modes should be higher than the reference spectrum for observations after April 2010. This effect is not observed and we believe that if the new photometric calibration is affected, the effect is within the uncertainties of the reference spectrum.

3. Bad Pixel Tables

In creating and testing the PHT and ripple tables, additional improvements were made to the FUV and near ultraviolet (NUV) bad pixel tables. The NUV and FUV bad pixel tables list the x- and y-pixel location of bad pixels on the detector and label them with a data quality flag. In the past, a single table was made for an entire detector and so grating specific bad pixels could not be identified. The format of the bad pixel table has been changed, adding an OPT_ELEM column. Values of a single grating or 'ALL' can be used in this column to specify grating specific bad pixels.

3.1 NUV Bad Pixel Table

The NUV detector suffers from vignetting in the corners of the detector which varies with grating. Previous bad pixel tables contained no information on the vignetting of the grating used in the observation. Instead it was marked in the flat field as seen by the G230M grating. The vignetted corners of each grating were characterized as described in Hart & Bostroem (2012) and added to the NUV bad pixel table. The data quality flag 64 was defined for these regions. A new NUV bad pixel table was delivered to the Calibration Database System (CDBS) and installed in the On-the-Fly Recalibration (OTFR) on March 01, 2011 (v2s21472o_bpx.fits).

3.2 FUV Bad Pixel Table

The FUV detector has a repeller wire which casts a shadow on the detector that depends on the light path and therefore the grating. Previous versions of the FUV bad pixel table marked the repeller wire at its location in the G140M grating for all gratings. The STIS Instrument Design Team (IDT) has identified the location of the repeller wire in each grating. These locations were added to the existing FUV bad pixel table to make a grating-dependent bad pixel table. The FUV bad pixel table was delivered to CDBS and installed in the OTFR on December 14, 2010 (uce15153o_bpx.fits).

4. Creation of the PHT and Ripple Tables

The echelle blaze function has been found to shift over time and with detector location. The shape of the blaze function is used in both the flux calibration (in the PHT tables) and in the 2D echelle scattered light background subtraction algorithm (in the ripple tables). These two files should always be created and used together. The coefficients used to characterize the shift with location and time are also found in the PHT table (BSHIFT_VS_X, BSHIFT_VS_Y, BSHIFT_VS_T, BSHIFT_OFFSET). The PHT and ripple tables are made by first determining a smooth sensitivity curve for each order. This curve is then normalized to create the ripple tables and is scaled and converted to efficiency units for the PHT tables.

4.1 Sensitivity Files

The sensitivity (S(λ)) of each order for each central wavelength is derived following the procedures described in Bohlin (1998). The data are calibrated with **calstis** (version 2.36) and the net counts and wavelengths are extracted from the one-dimensional spectral extraction files (dataset_x1d.fits). The net counts are then divided by the G191-B2B model flux spectrum (g191b2b_mod_007.fits) in the CDBS Calspec library, interpolated to the x1d wavelengths. A multi-node, least-squares cubic spline fit is made to the sensitivity curves of each order. Some large absorption features (e.g., Lyman α) are masked

while smaller features are extrapolated over. As the vignetting can shift slightly between observations, the bad pixel table cannot accurately mark the edges of the vignetted regions. For this reason the vignetting in some observations is explicitly marked with a data quality flag of 64 (obb002060_x1d.fits, obb053080_x1d.fits, obb053090_x1d.fits). These modifications allow the fit to follow the true sensitivity curve and not be made artificially low. Nodes are placed at uniform pixel locations in the cross-dispersion direction. A spline fit is performed both across an order (in the dispersion direction) and along a given node number (in the cross dispersion direction). When more than one observation of a given central wavelength is present, each observation is fit independently, then the observations are combined, weighted by their exposure time. Additional details on this procedure can be found in Bohlin (1998) and Aloisi et al (2007). A sensitivity file for each central wavelength is written containing the node locations in wavelength space and sensitivity values for each order.

When the last PHT tables were created some of the data came from extreme MSM offset positions. This placed some orders on the detector which are not normally visible at the nominal MSM offset position and others orders off the detector which are visible at the nominal MSM offset position. **calstis** currently does not calibrate orders not in the PHT tables even if they are on the detector and in the extraction table. This can be overridden by setting the header keyword FLUXCORR to OMIT in the dataset_raw.fits files and then recalibrating the data. In order to extract all orders falling on the detector in the 11866 observations two sets of sensitivity files are created; one from the standard calibration and one from the FLUXCORR = OMIT calibration. Orders which are well calibrated and fully on the detector but not in the old PHT table are copied from the FLUXCORR = OMIT sensitivity files into the sensitivity files from the standard calibration and used to make the PHT table.

Since the data in 11866 were taken at a single (nominal) MSM position, some orders which appeared in previous PHT tables will not be in these PHT tables. While this should have a minimal effect on data taken after SM4 at the nominal offset, **calstis** is being modified to handle and extract all orders on the detector which are in both the ripple table and the extraction table. For orders which are not in the PHT table, a value of 0 will be inserted into the FLUX and ERROR columns. A new column will be added to the dataset_x1d.fits files to report the error in units of count rate. This new behavior will be available in **calstis** version 2.37.

4.2 Initial PHT Table

The PHT table is used to convert extracted net counts to flux in the dataset_x1d.fits tables. To convert the sensitivity in the files created in the previous section into a PHT table, the TDS must be removed and the result extrapolated to an infinite aperture and converted to units of efficiencies.

The response of the STIS detector to light decreases over time. This effect is characterized in the TDS reference file (FUV: u7c1846ho_tds.fits, NUV: ub920085o_tds.fits).

Table 1. Orders with Negative Efficiencies

Grating	Central Wavelength	Order	Zeroed Wavelengths
E140M	1425	129	$\lambda < 1142.58$
E230M	2124	118	$\lambda < 1715.80$
E230M	2415	101	$\lambda < 2003.89$

The reference files are used to remove the TDS and correct the sensitivity to a reference time (the beginning of STIS operations in February 1997). No time-dependent temperature correction is applied.

Sensitivities are derived in units of (counts/s)/(ergs/cm^2/s/Å) and correspond to the telescope throughput measured in a 0.2″x 0.2″aperture with a standard 7 pixel extraction box. To generalize the measurement for use in **calstis** with any aperture and extraction box, the sensitivity must be converted to an efficiency for an infinite aperture and infinite extraction box. Efficiency is defined as:

$$\epsilon(\lambda) = S(\lambda)\frac{hc}{\lambda}\left(\frac{d\lambda}{dx}\right)^{-1}\frac{1}{A_{Tel}} \quad (1)$$

Where:
$S(\lambda)$ = wavelength dependent sensitivity
$\left(\frac{d\lambda}{dx}\right)$ = dispersion
A_{Tel} = the area of the telescope

The aperture and extraction box corrections are performed using standard reference files. These same files are used when converting the throughput curve back to a given aperture. Therefore, for observations using the same extraction height and aperture as the observations in 11866, there should be no error introduced with this extrapolation. However, flux values for observations performed with other apertures or reduced using other than the default extraction box height will be affected by any differential errors in the tabulated values of these corrections.

For a few orders, the efficiency dips to negative values. For these orders, the first negative wavelength when searching from the middle of the order is identified and the efficiency of all exterior wavelengths is set to zero. **calstis** will set the flux to zero for these wavelengths in these orders. The affected orders can be found in Table 1.

4.3 Ripple Table

The initial PHT tables are used to create the ripple tables. The ripple tables are used in the **calstis** routine **sc2d**. A two dimensional scattered light model is constructed by

Table 2. Orders which turn up at the edges

Grating	Central Wavelength	Order	Wavelength of inflection	Correction Applied
E230M	2269	109	$\lambda < 1858.71$	Extrapolate
E230M	1978	121	$\lambda > 1700.21$	No Correction
		122	$\lambda > 1685.58$	No Correction
		123	$\lambda > 1671.70$	No Correction
		124	$\lambda > 1658.32$	No Correction
		126	$\lambda > 1631.23$	No Correction
E230M	2124	119	$\lambda < 1703.20$	Extrapolate
			$\lambda > 1726.84$	Constant

sc2d and subtracted from the _flt image. The ripple table is used to flatten out the orders so that they can be spliced together into a single spectrum (see Valenti et al. 2002 for more details). For a given central wavelength, an eight node quartic least-squares univariate spline is fit to the peak of each order. A 9th order polynomial is also fit. At the edges of the full wavelength range of a central wavelength the spline and polynomial fit are evaluated by eye and one is chosen to fit the region outside the intersection of the spline and polynomial fit. The middle of the wavelength range is always fit with a spline. This fit is then used to normalize each order to a peak of ~ 1. For edge orders where the sensitivity declines steeply, the normalization can introduce an error in the shape of the blaze function. For this reason, the edge orders are inspected and replaced by a neighboring order if needed. Appendix B details which function was chosen to normalize each central wavelength (Table B.1) and which orders were replaced (Table B.2).

The sensitivity of some orders appears to turn up at the edges (see Figure 1. This is often an artificial effect of the noise at the edge of the detector. For this reason if a turn-up is found it can be corrected with an extrapolation based on the local linear fit, be extended at a constant sensitivity value from the wavelength of lowest sensitivity, or it can remain unchanged. Based on the shape of the net counts spectrum, a decision is made about each turn-up and the table is modified in place. Table 2 lists the orders which turn up and how they were modified.

A few edge orders have systematically high ripple curves when compared to neighboring orders. The curves of these orders were multiplied by the values specified in Table 3. The sensitivity of E230M/2415 order 102 was manually fit and renormalized.

The new NUV and FUV PHT tables (vb816447o_rip.fits and vb816446o_rip.fits respectively) were delivered to CDBS and installed in the OTFR on November 8, 2011.

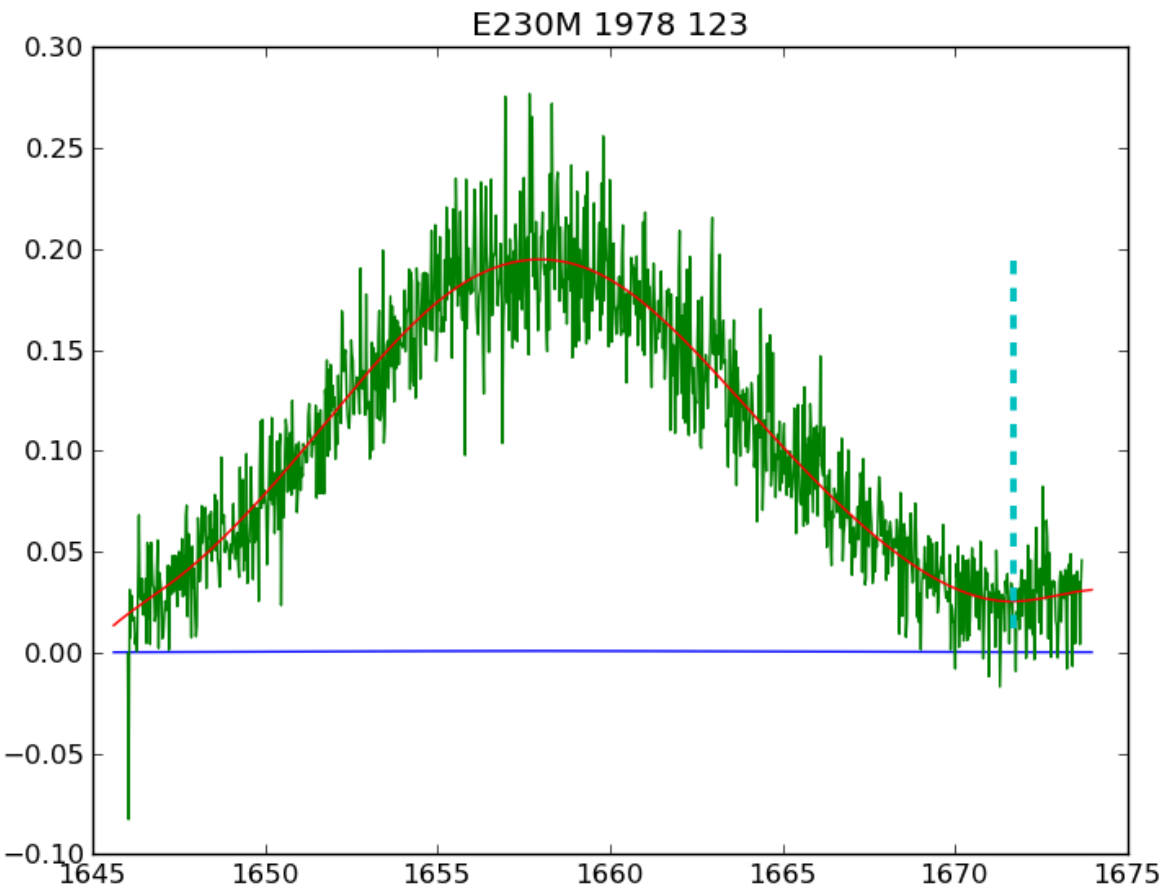

Figure 1. The net counts of G191-B2B observed with the E230M/1978 setting. Only order 123 is shown in green. The derived sensitivity is arbitrarily scaled to the peak of the net counts and plotted in red. The turn up occurs to the right of the dashed cyan line. In this case it was determined that the turn up occurs in the data and should be kept.

Table 3. Renormalized Orders

Grating	Central Wavelength	Order	Renormalization Factor
E230M	2415	100	0.9659
E230H	2912	278	0.9558
E230H	2713	273	0.9755
E230H	2663	277	0.9697
E230H	2563	287	0.9623
E230H	2213	330	0.9477
E140H	1562	255	0.9025

4.4 Final PHT Table

As the ripple table is used for background subtraction, a new ripple table can affect the net counts extracted. For this reason all of the data are recalibrated with the new ripple tables and new PHT tables are derived using the method described in Section 4.2. The spatial coefficients (BSHIFT_VS_X and BSHIFT_VS_Y) of the blaze function shift (BSHIFT) are not modified as they do not change with time. However, the temporal components are set to 0. BSHIFT_VS_T is set to 0 as Δt is very small. BSHIFT_VS_OFFSET is set to 0 as the PHT table is made with post-SM4 observations.

There are a few edge orders which when calibrated with the new PHT table, yield very inaccurate fluxes. E230H/2912 order 278 is poorly fit by the automated program, creating an artificially high sensitivity. This order is uniformly scaled to the correct sensitivity value. The nodes in the sensitivity curve fit to E230H/2513 order 324 are incorrectly smoothed in the cross-dispersion direction. For this order the fit prior to the cross-dispersion smoothing is used.

The new NUV and FUV PHT tables (vb816448o_pht.fits and vb816445o_pht.fits, respectively) were delivered to CDBS and installed in the OTFR on November 8, 2011.

4.5 Missing / Additional Orders

As previously mentioned, all observations for this calibration were taken at the nominal MSM monthly offset position. While the nominal position is now the default setting for all post-SM4 echelle observation, the non-repeatability of MSM position may cause some orders to slip on and off the detector. These orders cannot be calibrated with the current reference files. Appendix C Table C.1 details the orders which are in the previous PHT tables and are not currently in the new PHT tables as well as the orders which were not in the previous PHT tables but are in the current ones. Appendix C Table C.2 details the orders which were in the previous ripple tables and are not currently in the new ripple tables as well as the orders which were not in the previous ripple tables but are in the current ones.

Users working with data containing orders not calibrated with the new reference files may still be interested in extracting and calibrating these orders. If this is the case, they may resort to older versions of the tables with the caveat that the temporal component of the blaze-shift correction is not optimal for post-SM4 data.

5. Results and Accuracy

The uncertainties in the flux calibration of data calibrated with the new PHT, ripple, and bad pixel tables is evaluated by calculating the RMS scatter of flux of the program 11866 data around the Calspec model spectrum of G191-B2B. The median value of all observations is 2%. The same calculation performed on data calibrated with the old

tables yields a median uncertainty of 5%. Most of the improvement is due to a better post-SM4 blaze function characterization in the new throughput curves. Figure 2 shows an example of a portion of an E140H spectrum using the old reference files (in red), the new reference files (in green), and the reference spectrum (in black). The largest difference between the two calibrations can be seen in the alignment of the edges of the orders. The slant of each order of the old reference file calibrated data is indicative of a poor characterization of the shift of the post-SM4 blaze function when using the pre-SM4 photometric calibration. The Calspec model of G191-B2B has a systematic uncertainty of 4% in the UV (Bohlin 2007), which when summed in quadrature with the uncertainties in the flux calibration leads to an absolute flux calibration accuracy of 5%.

In the two years since program 11866 executed, the temporal component of the blaze function shift has continued to evolve. Figure 3 shows the evolution of the blaze function with time for the E230H grating which shows the fastest evolution of the shift of the blaze function of all of the echelle gratings. These changes continue to be monitored and new PHT tables with new temporal components for the blaze function shift will be delivered as needed. The effect is still less than 5% at this time.

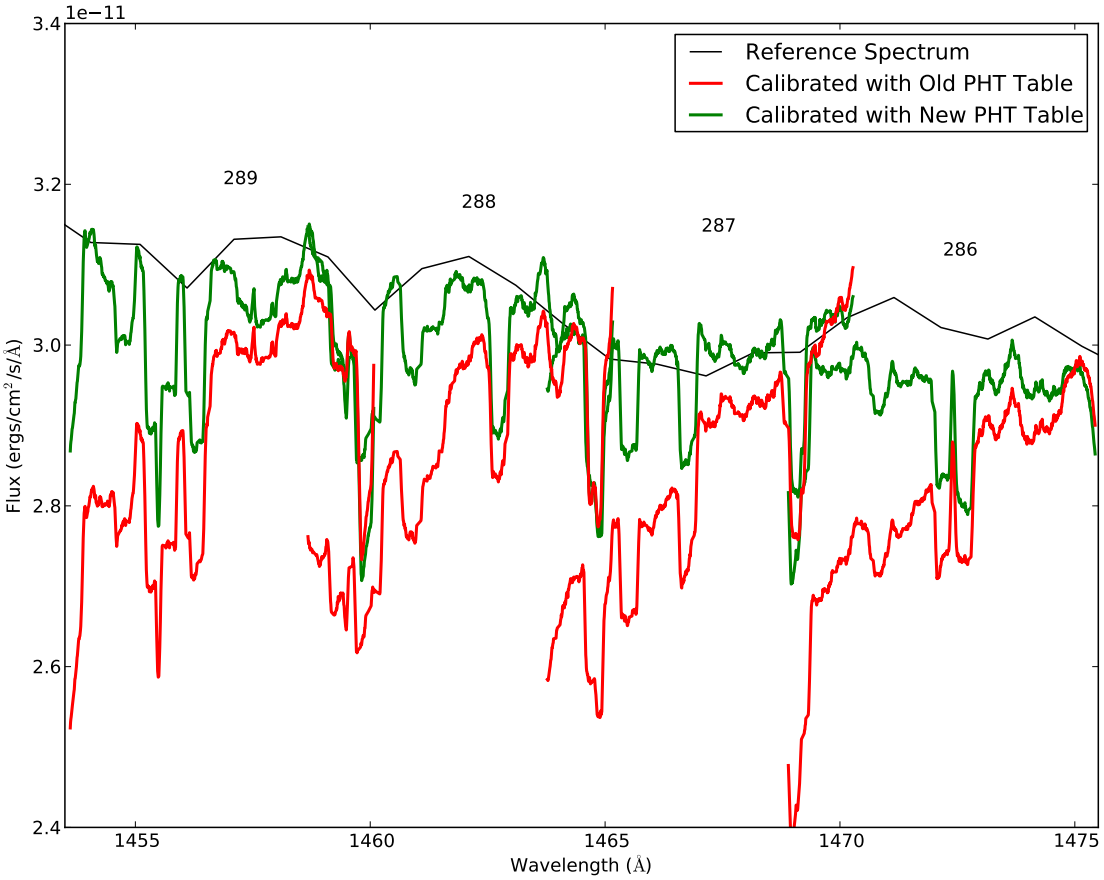

Figure 2. The spectrum of the HST secondary standard star BD+28D4211 calibrated with the new ripple and PHT tables (green) and the old ripple and PHT tables (red). The low resolution reference spectrum in is black. This observation was taken in June 2010 in the E140H/1416 Å mode as part of the standard TDS monitoring program. Only orders 286 - 289 are plotted. The slope of each order in the spectrum calibrated with the old reference files is indicative of a shift in the blaze function with time that is not properly calibrated after SM4 with the old (pre-SM4) photometric calibration. Both calibrations lie slightly below the reference spectrum indicating the need for new TDS reference files. The low calibrated flux is not due to the E140H anomaly affecting the photometric calibration data as the anomaly would produce a flux which is higher than the reference spectrum.

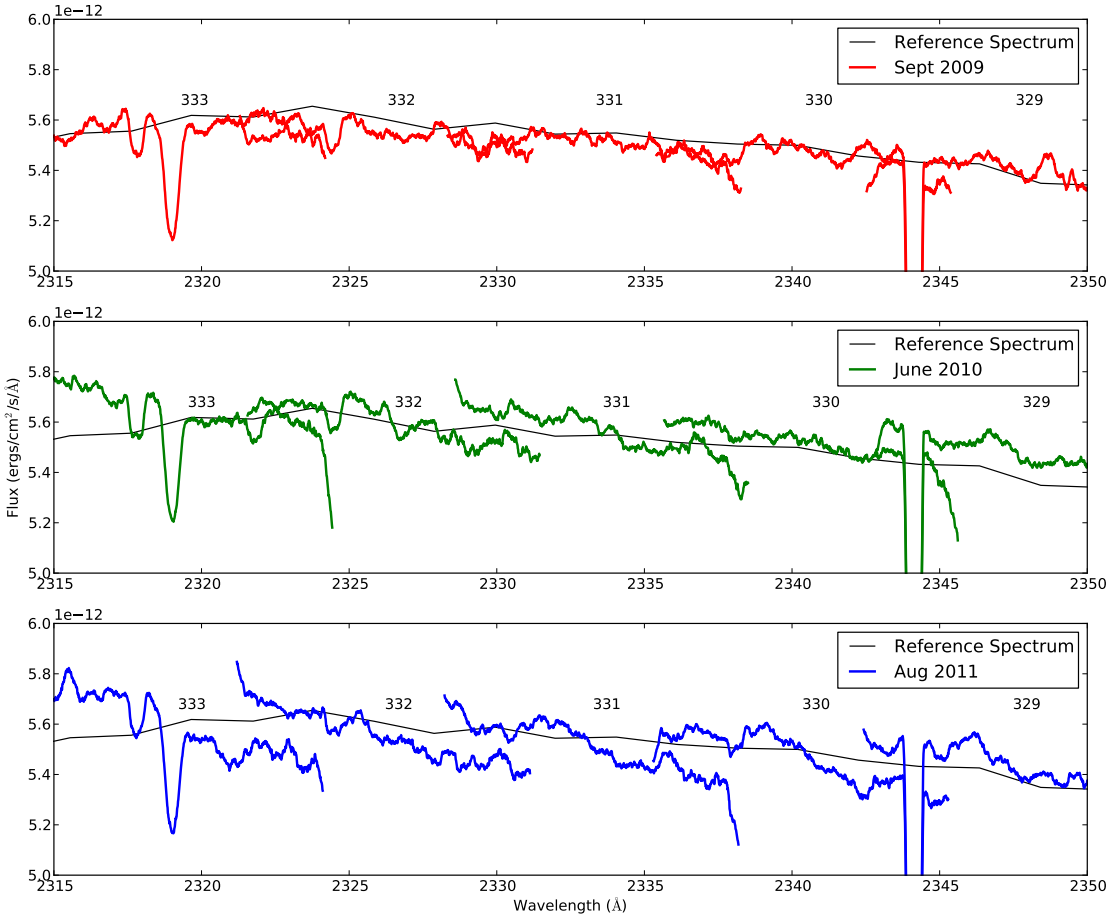

Figure 3. The spectrum of the HST secondary standard star BD+28D4211, taken with the E230H/2263 setting, calibrated with the new PHT and ripple tables. The top panel shows data taken in September 2009, the middle shows data taken in June 2010, and the bottom panel shows data taken in August 2011. While the orders are continuous in the Sept 2009 data, the blaze function evolution is apparent by June 2010 in the tilt of each order. This trend continues in the August 2011 data. This mismatch is still less than 5%. A new characterization of the blaze function shift with time for operations on Side-2 after the STIS repair will be performed in the near future.

References

Aloisi, A. 2005, in The 2005 HST Calibration Workshop Proceedings, p. 190 ed. A. M Koekemoer et al.
Aloisi, A.; Bohlin, R.; Quijano, J. K., 2007, STIS Instrument Science Report 2007-01
Aloisi, A. 2011, STIS Instrument Science Report 2011-04
Bohlin, R. C. 1998, STIS Instrument Science Report 1998-18
Bohlin, R. C. 2007, in The Future of Photometric, Spectrophotometric, and Polarimetric Standardization, ASP Conf. Series, Vol. 364, p. 315 ed. C. Sterken; also Astro-Ph 0608715
Hart, K. & Bostroem, K. A., 2012 (in prep)
Stys, D. J., Bohlin, R. C., & Goudfrooij, STIS Instrument Science Report 2004-04
Valenti, J. A., et al. 2002, STIS Instrument Science Report 2002-01

Appendix A

The Echelle Blaze Function Shift

The echelle blaze function depends on both the location of the spectrum on the detector and time. Changes to angle of incident light on an echelle grating causes the spectrum to shift locations on the detector and the grating efficiency curve (or grating blaze) to independently shift (see Lindler & Bowers, 2002). This is the so-called blaze function shift. The spatial component of the blaze function shift is caused by changes in the location of the spectrum on the detector due to the non-repeatbility of the mode select mechanism and the mode select mechanism offsetting (Lindler & Bowers, 2002). The temporal component of the blaze function shift is caused by shifts in the angle of the grating grooves over time (Lindler & Bowers, 2002). The temporal and spatial components combine to shift the efficiency curve linearly based on the x and y location of the spectrum on the detector and the time of the observation. The blaze function shift in pixels is defined as

$$BSHIFT = BSHIFT\_VS\_X \times \Delta x + SHIFT\_VS\_Y \times \Delta y + BSHIFT\_VS\_T \times \Delta t + BSHIFT\_OFFSET \tag{A.1}$$

BSHIFT_VS_T and BSHIFT_OFFSET describe the temporal component of the blaze-shift which varies with grating, order, and side of STIS operations, while BSHIFT_VS_X and BSHIFT_VS_Y describe the spatial component which varies with grating used.

The coefficients BSHIFT_VS_X, BSHIFT_VS_Y, BSHIFT_VS_T, and BSHIFT_OFFSET are stored in the Photometric Conversion (PHT) Table. Also stored in the PHT table are a reference spectra characterized by a reference order number, REFWAVE, the wavelength value at the pixel 512 in the reference order, and REFY, the extraction location of the pixel 512 in the reference order, and REFMJD, the modified julian date of the median exposure used to infer the echelle sensitivity. When an observation occurs, OBSW, the observed wavelength in the reference order at the pixel 512 is found as well as OBSY, the average y offset of the pixel 512 over all orders. These values are used to

define Δ x, Δ y, and Δ t as follows:

$$\Delta x = (REFWAVE - OBSW)/dispersion$$
$$\Delta y = OBSY - REFY$$
$$\Delta t = OBSDATE - REFMJD$$

BSHIFT is then calculated, converted to wavelengths using the dispersion, scaled by the reference order divided by the current order, and added to the sensitivity wavelengths for the current order.

Appendix B

Ripple Table Special Fitting

Table B.1.: Fits to the peaks of orders for each central wavelength used for normalizing the sensitivity curves for making the ripple tables.

Grating	Central Wavelength	Left Edge Fit	Right Edge Fit
	FUV-MAMA		
E140M	1425	p	s
E140H	1416	s	s
	1562	s	s
	1307	s	s
	1453	p	p
	1343	p	s
	1234	s	p
	1380	s	s
	1489	p	p
	1598	s	s
	1526	s	s
	1271	s	p
	NUV-MAMA		
E230M	2561	s	s
	2707	p	p
	2269	s	s
	1978	s	s
	2124	s	s
	2415	s	s
E230H	2563	s	p
	2313	s	p
	2063	s	s
	2962	p	p
	1813	p	p
	2713	p	p
	2463	s	p
	2213	p	p
	1963	s	p
	2862	p	p
	2613	s	s
	2363	s	p
	2113	s	s

Continued on Next Page . . .

Table B.1 –Continued

Grating	Central Wavelength	Left Edge Fit	Right Edge Fit
	3012	p	p
	1863	p	p
	2762	s	p
	2263	p	p
	2013	s	p
	2912	p	p
	1763	p	p
	2513	p	p
	2663	s	p
	2413	s	p
	2163	s	p
	1913	p	p
	2812	s	p

Table B.2.: Orders where the ripple function was replaced by the ripple function of a neighboring order in the ripple tables.

Grating	Central Wavelength	Replaced Order	Replacement Order
		FUV-MAMA	
E140M	1425	129	128
	1425	128	127
	1425	88	89
E140H	1416	279	280
	1562	256	257
	1562	255	256
	1307	303	304
	1453	272	274
	1343	338	337
	1234	368	366
	1234	367	366
	1380	287	288
	1380	286	287
	1489	303	302
	1489	266	267
	1598	281	280
	1598	251	252
	1526	295	294
	1526	261	262
	1526	260	261
	1271	311	312
		NUV-MAMA	
E230M	1978	126	124
	2269	109	108

Continued on Next Page . . .

Table B.2 –Continued

Grating	Central Wavelength	Replace Order	Replacement Order
	2415	102	100
E230H	2962	250	251
	2713	299	298
	2463	331	330
	2213	371	370
	2213	330	331
	1963	368	369
	2113	389	388
	2113	343	344
	3012	246	247
	1863	446	445
	2762	268	269
	2263	322	323
	2013	410	409
	2912	254	255
	1763	473	472
	2513	324	323
	2663	277	278
	1913	378	379

Appendix C

Missing / Additional Orders in the PHT and ripple tables

Table C.1.: Missing / additional echelle orders in the new PHT tables

Grating	Central Wavelength	Missing	Additional
	FUV-MAMA		
E140H	1234	316	...
	1271	363, 362	...
	1307	...	...
	1343	339	...
	1380	329	...
	1416	319, 278	...
	1453	310	...
	1489	265	303
	1526	259	295
	1562	254	...
	1598	282	...
E140M	1425	86	...
	NUV-MAMA		
E230H	1763	407, 406	...
	1813	459	...
	1863	447	...
	1913	434	...
	1963	421	...
	2013	411	...
	2063	400, 399	...
	2113	390	343
	2163	381	336
	2213	372	...
	2263	363	...
	2313	356, 355	316
	2363	347	...
	2413	...	...
	2463	297	...
	2513	...	...
	2563	286	...
	2613	281	...
	2663	276	...
	2713	272	...

Continued on Next Page ...

Table C.1 –Continued

Grating	Central Wavelength	Missing	Additional
	2762	267	...
	2812	263	...
	2862	258	...
	2912	253	278
	2962	...	...
	3012	268	...
E230M	1978	86	...
	2124	120	...
	2269	110	...
	2415	103, 73	...
	2561	95	...
	2707	66	...

Table C.2.: Missing / additional echelle orders in the new ripple tables

Grating	Central Wavelength	Missing	Additional
	FUV-MAMA		
E140H	1234	316	...
	1271	309, 310, 362, 363	...
	1307	300, 301, 352	...
	1343	291, 292, 339	...
	1380	284, 285, 329	...
	1416	319, 278	...
	1453	270, 271, 310	...
	1489	265, 304	...
	1526	259, 296	...
	1562	253, 254, 288, 289	...
	1598	249	...
E140M	1425	...	129
	NUV-MAMA		
E230H	1763	474, 407	...
	1813	394, 395, 459	...
	1863	384, 385, 386, 447	...
	1913	375, 376, 434	...
	1963	365, 366, 367, 421	...
	2013	359	...
	2063	349, 350, 399, 400	...
	2113	342, 390,	...
	2163	335, 381	...
	2213	328, 329, 372	...
	2263	...	...
	2313	315, 355, 356	...
	2363	308, 309, 347, 348	...

Continued on Next Page ...

Table C.2 –Continued

Grating	Central Wavelength	Missing	Additional
	2413	302, 303, 340	...
	2463	296, 297, 332, 333	...
	2513	291	...
	2563	285, 286, 318, 319	...
	2613	280, 281, 311, 312	...
	2663	276, 306, 307	...
	2713	271, 272, 300, 301	...
	2763	...	...
	2812	262, 263, 290	...
	2862	257, 258, 284	...
	2912	253, 279	...
	2962	249, 274	...
	3012	245	...
E230M	1978	...	...
	2124	80, 81, 120	...
	2269	75, 76, 110	...
	2415	72, 73, 103	...
	2561	68, 69, 95	...
	2707	66	...